

Creep in carbonatable binders Investigating non-hydraulic lime mortars

da Silva Munhoz, Guilherme; Ye, Guang

10.1016/j.conbuildmat.2025.143751

Publication date

Document Version Final published version

Published in

Construction and Building Materials

Citation (APA)

da Silva Munhoz, G., & Ye, G. (2025). Creep in carbonatable binders: Investigating non-hydraulic lime mortars. Construction and Building Materials, 496, Article 143751. https://doi.org/10.1016/j.conbuildmat.2025.143751

Important note

To cite this publication, please use the final published version (if applicable). Please check the document version above.

Other than for strictly personal use, it is not permitted to download, forward or distribute the text or part of it, without the consent of the author(s) and/or copyright holder(s), unless the work is under an open content license such as Creative Commons.

Takedown policy

Please contact us and provide details if you believe this document breaches copyrights. We will remove access to the work immediately and investigate your claim.

ELSEVIER

Contents lists available at ScienceDirect

Construction and Building Materials

journal homepage: www.elsevier.com/locate/conbuildmat



Creep in carbonatable binders: Investigating non-hydraulic lime mortars

Guilherme da Silva Munhoz *0, Guang Ye

Delft University of Technology, Stevinweg 1, Delft 2628 CN, the Netherlands

ARTICLE INFO

Keywords: Carbonatable binder Non-hydraulic lime Air lime Characterization Creep

ABSTRACT

Non-hydraulic lime (also known as air lime) is an ancient carbonatable binder that has regained attention due to its carbon sink potential. Besides lower CO₂ emissions during production, air lime also absorbs carbon dioxide during its hardening process. Yet, the challenge with non-hydraulic lime (and alternative binders in general) lies in the absence of data, standards, and replicable studies. For instance, air lime is often used in masonry mortars, where volume stability (shrinkage and creep) is required to ensure structural safety, but research on this issue remains scarce. Therefore, the objective of this study was to apply existing frameworks to experimentally measure the total creep (EN 12390-17:2019) of non-hydraulic lime-containing mortars. Four groups were analyzed, with non-hydraulic lime contents of 100 %, 67 %, 50 %, and 0 % (binder volume). Specimens were subjected to three different curing conditions and then loaded and monitored for up to 240 days. The results showed that (i) unlike Portland cement, non-hydraulic lime mortars needed more time to develop strength under natural environmental conditions; (ii) the phenolphthalein test did not accurately monitor the carbonation depth of air lime-rich mortars; (iii) air lime-rich systems showed less shrinkage, possibly due to carbonation-induced expansion; and (iv) air lime-rich groups exhibited greater creep strains, confirming their high deformability. These findings demonstrate that air lime-containing mortars exhibit a distinct time-dependent behavior, highlighting the need to adapt existing standards for more accurate and reproducible long-term performance assessments.

1. Introduction

Lime, a carbonatable binder, has been used as a building material for thousands of years. Some studies indicate that lime-based applications first emerged in the Middle East (7000 BCE), followed by Asia (2000 BCE) and South America (500 BCE) [1,2]. Significant advancements in lime-based practices were made by the Phoenicians, Greeks, and Romans, with techniques gradually evolving across civilizations until the creation of Portland cement in the 19th century. At that point, the decline of lime became inevitable, since Portland cement could overcome many of the limitations associated with the non-hydraulic binder, including slow setting and low mechanical strength [3,4].

Today, two centuries later, lime is trending once again. As environmental regulations urge the construction industry to reduce Portland cement production (due to its significant carbon dioxide emissions), several alternative binders have been explored, including lime, limestone calcined clay, and alkali-activated materials [5–7]. Lime's lower calcination temperature (compared to Portland cement) and its capacity to absorb carbon dioxide make it a promising candidate for

decarbonizing the building sector. This study focuses on air lime, a subtype particularly relevant because its hardening relies exclusively on carbon dioxide sequestration.

Even though air lime is not a newly developed binder, it faces challenges similar to those of emerging materials: limited scientific consensus on its short- and long-term properties [3], and the absence of standards capable of assessing its performance [8]. These issues are largely rooted in the fact that expertise associated with air lime applications was predominantly empirical and has gradually been lost over time. Consequently, fundamental studies characterizing this binder from different perspectives (i.e., physical and mechanical) remain in demand [9].

Recent studies, such as those by Oliveira *et al.* [9] and Branco *et al.* [10], investigated the physical properties of hardened air lime mortars. Similarly, the strength development of air lime-containing mortars was addressed by Oliveira *et al.* [9] and Kang *et al.* [11]. Blended systems (such as air lime-pozzolana [12,13] and white Portland cement-lime mortars [3,8]) and the influence of aggregate type [14] have also been explored. However, only few papers have focused on the volume

E-mail address: g.dasilvamunhoz-1@tudelft.nl (G. da Silva Munhoz).

^{*} Corresponding author.

stability of air lime-containing mortars. In this study, volume stability is treated as a physicomechanical phenomenon characterized by shrinkage (length change due to intrinsic and extrinsic factors) and creep (time-dependent deformation under constant load and defined conditions). Among them, creep remains one of the least investigated and most underestimated aspects of air lime-containing mortars [15,16] and is the focus of this research.

To the best of the authors' knowledge, only one study has investigated the creep behavior of air lime-containing mortars in the last decade. In 2015, Macharia [15] measured creep in small air lime-cement mortar cylinders and concluded that the air lime content is directly proportional to creep strains, highlighting the need for further research on the topic. Earlier studies from 2004, including those by Brooks and Bakar [16] and Papayianni [17], had already raised similar concerns, noting that excessive creep can compromise durability and structural integrity [9,14]. These issues are especially critical in applications where air lime is extensively used, such as the conservation of built heritage and masonry systems.

In conservation technology, inaccurate assumptions about deformation behavior may lead to the failure of delicate retrofitting systems, incompatibility with adjacent materials, and accelerated deterioration resulting from cracking. In masonry systems, the creep of lime mortars is often overlooked based on the assumption that the influence of the mortar joint is negligible, given its relatively small volume compared to the masonry units [16]. This assumption often lacks validation and underestimates long-term displacements, an issue that has been linked to partial and full collapse of buildings, as documented in the literature [16,18].

Therefore, there is an urgent need to develop robust, reproducible knowledge on the creep behavior of air lime-containing mortars to support the dissemination of air lime as a structurally viable and sustainable binder. In this context, the aim of this study was to measure the total creep of air lime-containing mortars for up to 240 days. Additional properties were also investigated, including compressive strength, Emodulus, length change, and carbonation depth. Due to the lack of standards specifically designed to evaluate total creep in non-hydraulic binders, the existing framework for Portland cement (EN 12390–17:2019 [19]) was adopted, along with the assumptions it entails.

2. Materials and methods

2.1. Materials

To investigate the influence of air lime on the creep behavior of mortars, four mixtures were designed based on commonly employed formulations for masonry systems [13,14]. The materials included Portland cement with added limestone (CEM II/A–L 32.5 R), non-hydraulic lime (CL90S), standard siliceous sand (0–2 mm), and tap water. To ensure that all mixtures were suitable for the same intended application, the flow diameter was fixed at (164 \pm 7) mm, in accordance with the procedure specified in EN 459–2:2021 [20], a standard designed specifically for testing building lime. Further mixture details are provided in Table 1.

The chemical compositions of Portland cement and air lime were determined using XRF, and the results are presented in Table 2. The physical characteristics of the binders, including bulk density, specific gravity, and D_{50} (median particle size determined by laser diffraction) are presented in Table 3.

The mineralogical composition of the standard siliceous sand was determined using XRD (5°–75° scan range, 1.25 s counting time per step, $0.020^{\circ}~2\theta$ step size). No mineralogical phases other than quartz (SiO₂) were identified. The physical characteristics of the sand, including bulk density, specific gravity, and water absorption are shown in Table 4.

Regarding specimen production, all four mortar groups (Table 1) were prepared using the same procedure. Mixing lasted four minutes

Table 1Mixture design for masonry mortar applications.

Groups ^a	Cement (kg/m³)	Air Lime (kg/m³)	Sand (kg/m³)	Water (kg/m³)	Flow diameter (mm)
C100L0	340	_	1677	252	157
C50L50	176	65	1741	248	161
C33L67	118	86	1742	256	165
C0L100	_	131	1760	265	170

 $^{\rm a}$ C100L0 represents a mixture with 0 % of lime and 100 % of Portland cement; C50L50 represents a mixture with 50 % of lime and 50 % of Portland cement; C33L67 represents a mixture with 67 % of lime and 33 % of Portland cement; C0L100 represents a mixture with 100 % of lime and 0 % of Portland cement. Calculated based on the binder volume.

and was followed by casting in two layers. Each layer was compacted using mechanical vibration for 30 s, in accordance with the instructions provided in EN 459–2:2021 [20] and EN 196–1:2016 [21]. The environmental conditions for curing and storage (prior to the physical and mechanical tests) are described in the following subsection.

2.2. Methods

This study aimed to investigate the total creep of air lime-containing mortars under three different curing treatments. After casting, all specimens underwent an initial 7-day curing (common to all groups and treatments), after which they were divided into three curing treatments (A, B, and C). In treatments A and B, specimens were cured for 28 and 91 days, respectively, at 0.04 % CO₂. In treatment C, specimens were cured for 28 days, at 1 % CO₂. During the initial 7-day curing, all groups were kept in a humid chamber (95 \pm 5) % RH, in accordance with EN 1015–11:2019 [22]. Each curing treatment is summarized in Fig. 1.

Before effectively addressing the creep behavior of air lime-containing mortars, complementary tests were required. First, compressive strength was measured, as it determines the creep load to be applied to the specimens. Second, length change was monitored in companion specimens so that it could be subtracted from the total strain recorded during creep monitoring. These steps are detailed in EN 12390–17:2019 [19].

Additional experiments, although not explicitly required by EN 12390–17:2019 [19], also provided valuable insights into the creep behavior of air lime-containing mortars. In this study, thermogravimetric analyses were conducted to assess the progress of carbonation and hydration over time; phenolphthalein aspersion was used to determine the carbonation depth of fractured specimens; and elastic moduli were measured to evaluate the elastic response of air lime. An overview of the experimental program is shown in Fig. 2. Further details about each experiment are provided in the following subsections.

2.2.1. Compressive strength

Compressive strength was determined using mortar cubes measuring $10 \times 10 \times 10$ cm (Fig. 3a). The cubes were tested at 28, 91, and 182 days after casting. The loading rates followed the procedures specified in EN 1015–11:2019 [22] and EN 12390–3:2019 [23]. Three replicates were tested per group (twelve per curing treatment). Each curing treatment (A, B, and C) was described in Fig. 1.

2.2.2. Length change

For the length change assessment, specimens measuring $10 \times 10 \times 40$ cm were used. Two replicates (four measuring points in total) were tested per group, resulting in eight per curing treatment. The preparation of the specimens is shown in Fig. 3b. Total displacement was manually recorded using dial gauges (± 0.001 mm) at the intervals recommended by EN 12390–16:2019 [24]. The full dataset, including additional intervals, is available in [25].

Table 2Chemical composition of the binders determined using XRF.

Binder	CaO (%)	SiO ₂ (%)	Al ₂ O ₃ (%)	Fe ₂ O ₃ (%)	SO ₃ (%)	MgO (%)	K ₂ O (%)	TiO ₂ (%)	Na ₂ O (%)	Others ^a (%)
Cement	73.16	15.44	3.67	3.13	2.54	0.92	0.37	0.28	0.19	0.30
Air lime	98.72	0.12	0.06	0.06	0.07	0.80	0.03	-	0.03	0.11

 $^{^{\}rm a}$ It may include negligible contents of P2O5, SrO, Cl, ZnO, MnO, BaO, ZrO2, PbO, Rb2O, and Y2O3.

Table 3Physical characterization of the binders.

Properties	Cement CEM II A/L 32.5 R	Hydrated Lime CL90S
Bulk density (kg/cm ³)	(1068.47 ± 4.36)	(391.69 ± 3.67)
Specific gravity (-)	(3135.72 ± 10.70)	(2176.88 ± 71.59)
D ₅₀ – Laser diffraction (µm)	26.23	10.54

Table 4Physical properties of the standard sand.

Material	Bulk density (kg/cm³)	Specific gravity (-)	Absorption (%)
Standard sand ^a	(1763.55 ± 14.64)	(2622.98 ± 27.63)	(0.07 ± 0.01)

 $^{^{\}rm a}$ The standard sand is in line with the recommendations from EN 196–1:2016 [21].

2.2.3. Creep testing: instantaneous strain, total strain, and total creep

Two replicates (four measuring points in total) were used to track instantaneous and total strain, which was later used to calculate total creep. The specimens were tested according to EN 12390–17:2019 [19], with all groups subjected to a constant load equal to 30 % of their 28-day compressive strength (treatments A and C) or 91-day compressive strength (treatment B). Specimens under treatment A were monitored for up to 56 days, while those under treatments B and C were monitored for 240 days. Total displacement was continuously measured using

automated LVDTs (\pm 0.0001 mm), and the full dataset is available in [26]. The test setup is shown in Fig. 3c.

2.2.4. Additional characterization experiments

In addition to the tests conducted as part of the creep investigation (compressive strength, length change, and total creep), additional experiments were planned to better understand the effect of carbonation on strength and deformation: phenolphthalein test, thermogravimetric analysis (TGA), and elastic modulus.

• Phenolphthalein test

A phenolphthalein solution (1 % in 70 % ethanol) was sprayed onto the freshly fractured surfaces of the $4\times4\times16$ cm specimens. The carbonation front was measured using a precision ruler (±0.25 mm). According to RILEM CPC-18 [27], a pH below 9 (colorless) indicates a carbonated zone, while a pH above 9 (shades of pink/fuchsia) indicates a non-carbonated zone. This test was repeated at 28, 91, and 182 days after casting.

• Thermogravimetric analysis (TGA)

Fragments of approximately 1 cm³ were extracted from the fractured surface of the specimens, at depths ranging from 5 mm to 15 mm, for the TG analysis. Pore water was removed using the solvent-exchange method, commonly adopted in the literature [11]. The samples were then dried and finely ground.

The testing protocol followed the recommendations of Lothenbach *et al.* [28]. Weight losses in the 350–500 $^{\circ}$ C range were attributed to the dehydration of calcium hydroxide, while losses in the 600–850 $^{\circ}$ C range were associated with the decarbonation of calcium

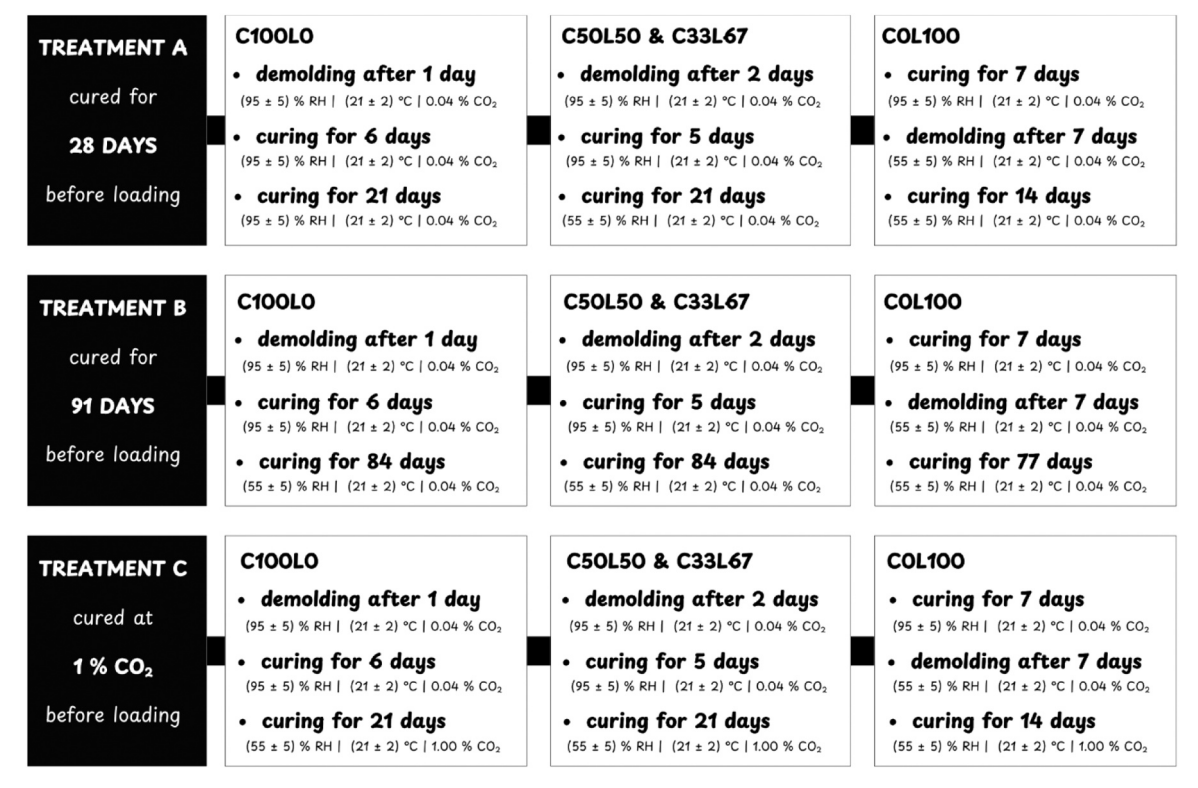


Fig. 1. Curing treatments A, B, and C (before the commencement of the experimental tests).

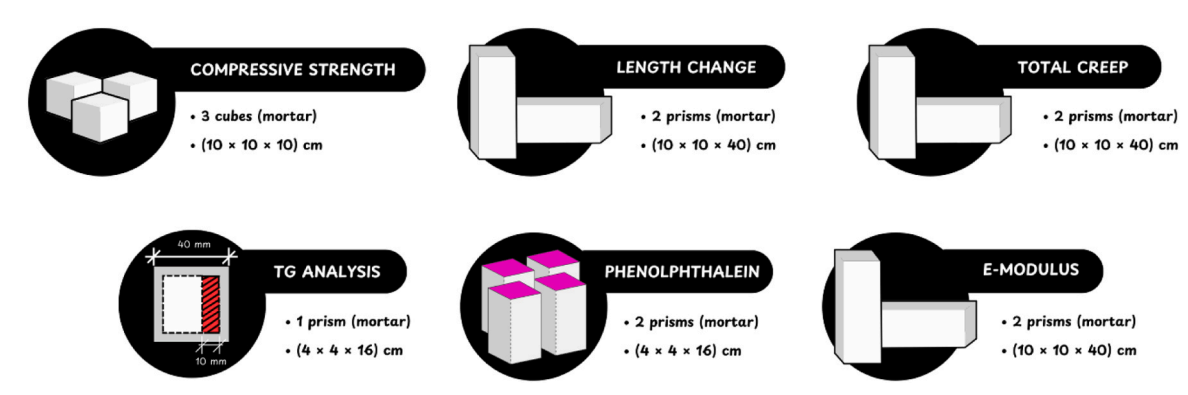


Fig. 2. Summary of the experimental program.

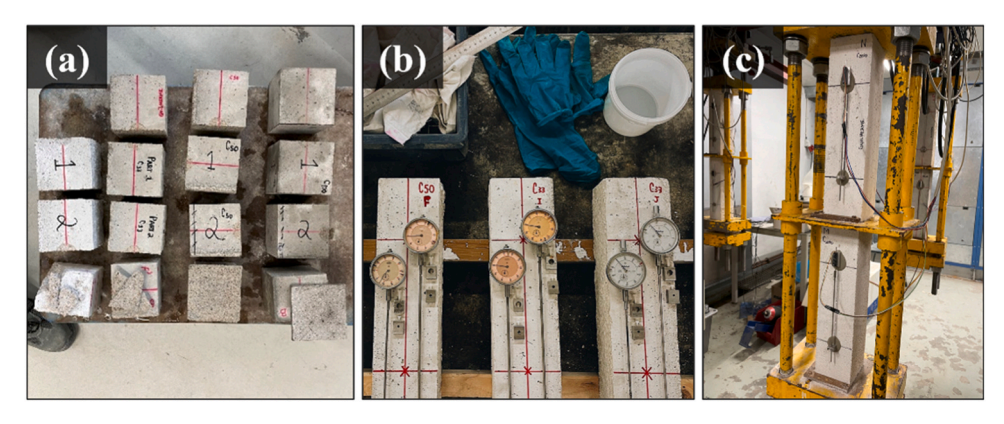


Fig. 3. Specimens for (a) compressive strength, (b) total shrinkage, and (c) total creep.

carbonate. Approximately 40 mg of powdered sample was heated from ambient temperature to $1000\,^{\circ}\text{C}$, at a heating rate of $20\,^{\circ}\text{C/min}$. An argon atmosphere was used to prevent any additional carbonation during the test. Measurements were conducted at 28, 91, and 182 days after casting.

• Elastic modulus

Additional prisms ($10 \times 10 \times 40$ cm) were cast to measure the stabilized secant modulus of elasticity of air lime-containing mortars. For each group, two replicates were tested using the loading-unloading Method B, specified in EN 12390–13:2021 [29]. Specimens were subjected to three loading cycles at 30 % of their compressive strength at 28 days (treatments A and C) or 91 days (treatment B). Displacements were measured using automated LVDTs (± 0.0001 mm) over a 100 mm gauge length. The mortar prisms were subjected to the same curing and storage conditions described in Fig. 1.

For conciseness, the results of these additional experiments (phenolphthalein, TGA, and elastic modulus) are presented in connection with the most relevant discussions throughout the paper, rather than in a separate section.

3. Results and discussions

3.1. Compressive strength and carbonation

The compressive strength of air lime-containing mortars was measured to assess their mechanical performance and to determine the reference load for the creep tests. The results are presented in Table 5.

Based on the results in Table 5, the groups cured for 91 days at 0.04 % CO₂ (treatment B) and those cured for 28 days at 1 % CO₂ (treatment C) exhibited higher compressive strengths than the groups cured for 28 days at 0.04 % CO₂ (treatment A). In all treatments,

Table 5Compressive strengths at 28 days (treatments A and C) and 91 days (treatment B).

Groups	Treatment A ^a (MPa)	Treatment Ba (MPa)	Treatment Ca (MPa)
C100L0	20.03 ± 0.32	24.77 ± 1.14	27.85 ± 0.28
C50L50	7.06 ± 0.55	7.80 ± 0.75	8.72 ± 0.08
C33L67	2.67 ± 0.13	3.32 ± 0.16	4.13 ± 0.02
C0L100	$\textbf{0.28} \pm \textbf{0.03}$	0.73 ± 0.05	1.00 ± 0.05

 $^{^{\}rm a}$ In treatments A and B, specimens were cured for 28 and 91 days, respectively, at 0.04 % CO2. In treatment C, specimens were cured for 28 days at 1 % CO2.

compressive strength decreased proportionally to the air lime content in the mixture. When comparing strength across treatments (Fig. 4), treatment C was the most effective, promoting both the fastest strength gain and the highest overall values. Treatment B yielded comparable strength levels, though over a significantly longer curing period (3 months).

The behavior observed in Table 5 and Fig. 4 suggests that carbonation is a slow mechanism under natural environmental conditions, requiring either extended curing times or exposure to increased $\rm CO_2$ concentrations to promote strength development. This hypothesis was confirmed by spraying phenolphthalein onto the freshly fractured surfaces of the specimens, which revealed a carbonation front consistent with this trend. The carbonation depth measurements are shown in Table 6.

As shown in Table 6, carbonation depth increased with the lime content. This trend can be explained by two main reasons: (i) lime-rich mixtures contain a higher amount of calcium hydroxide available, which increases the potential for carbonation; and (ii) air lime increases the overall porosity of mortars, which facilitates CO₂ ingress, as noted by Lanas *et al.* [30]. Treatment C exhibited the greatest carbonation depths,

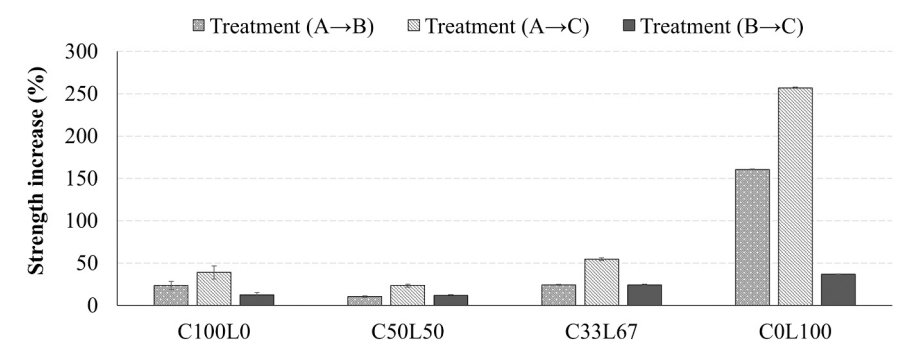


Fig. 4. Strength increases comparing different treatments.

Table 6
Carbonation depth at 28 days (treatments A and C) and 91 days (treatment B).

Groups	Treatment A (mm)	Treatment B (mm)	Treatment C (mm)
C100L0	2.42 ± 0.51	4.96 ± 0.43	$\textbf{7.87} \pm \textbf{0.28}$
C50L50	3.71 ± 0.54	9.27 ± 0.65	Fully carbonated ^b
C33L67	3.93 ± 0.51	10.50 ± 0.71	Fully carbonated ^b
C0L100	Indistinguishable ^a	Indistinguishable ^a	Fully carbonated ^b

^a Air lime-rich mixtures could not be measured, as their surfaces rapidly turned pink, suggesting a persistently high pH despite ongoing carbonation.

followed by treatment B, consistent with the trend previously observed in Table 5.

In treatments A and B, the carbonation depth of the pure lime mixture (C0L100) could not be determined with the phenolphthalein method. Although the freshly fractured surface initially showed a visible carbonation front, the entire section turned pink within seconds, preventing accurate measurement. Oliveira *et al.* [9] attributed this behavior to the formation of Liesegang rings.

Liesegang rings are localized patterns that arise due to differential conditions (e.g., moisture levels or calcium concentrations) promoting calcium carbonate precipitation at specific locations while inhibiting it at others. This mechanism explains the pink stains observed within the carbonated layer, shown in Fig. 5. Further details on Liesegang rings can be found in Rodriguez-Navarro *et al.* [31]. It should also be noted that the elevated pH of lime-rich systems may have influenced the effectiveness of phenolphthalein as a carbonation indicator, since this behavior was not observed in the pure cement group (C100L0).

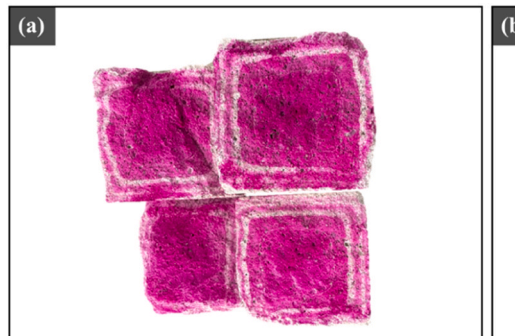
Given the limitations of the phenolphthalein test, thermogravimetric analysis was conducted to provide a more accurate assessment of the actual carbonation occurring in the specimens. The results for all treatments are presented in Fig. 6a-c.

According to Fig. 6a-c, the weight loss associated with the decarbonation of calcium carbonate was more substantial than that from the dehydroxylation of calcium hydroxide, suggesting that carbonation products represent a larger fraction of the samples. However, it is relevant to highlight that the mortar specimens were prepared with a cement containing added limestone (CEM II A/L). Consequently, the thermogravimetric results shown in Fig. 6a-c likely overestimate the decarbonation-related weight loss, since it is difficult to distinguish between carbonates originally present in the cement (limestone filler) and those formed through carbonation. To address this limitation, a semi-quantitative analysis was performed.

For the semi-quantitative analysis, the thermogravimetric data (Fig. 6a-c) were normalized to the binder fraction of each mixture. This approach was intended to enable a more consistent comparison across treatments by estimating the overall calcium hydroxide content relative to weight loss (Fig. 6) and mixture composition (Table 1). The calculations assumed a fixed 1:3 binder-to-aggregate volumetric ratio and used the experimentally measured densities of lime (2.08 g/cm³), cement (3.14 g/cm³), and siliceous sand (2.62 g/cm³). The results in Fig. 7a are presented in arbitrary units to illustrate trends rather than absolute Ca (OH)2 content.

A carbonation index was also calculated, as shown in Fig. 7b. It is defined as the ratio between the weight loss from $CaCO_3$ decarbonation and that from calcium hydroxide dehydroxylation. Although this approach cannot distinguish between carbonates originally present in the cement (limestone filler) and those formed through carbonation, it provides a useful indicator for comparing relative trends across mixtures. The index was normalized by the binder fraction of each group.

The results from Figs. 6 and 7 indicate that the pure lime group (COL100) carbonated over time, despite the inconsistencies observed with the phenolphthalein test. Moreover, while visual inspection suggested that some groups under treatment C were fully carbonated, TGA results revealed otherwise, confirming the presence of calcium hydroxide (Fig. 7a). These findings indicate that the phenolphthalein test can overestimate the degree of carbonation—particularly in air lime-containing groups. Thus, complementary techniques (e.g., TGA, FTIR, etc.) are recommended to ensure a more accurate assessment.



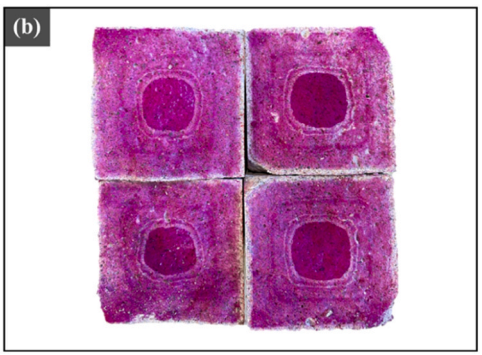


Fig. 5. Examples of indistinguishable carbonation front in lime-rich mortars.

^b The specimens were classified as fully carbonated based on a visual inspection.

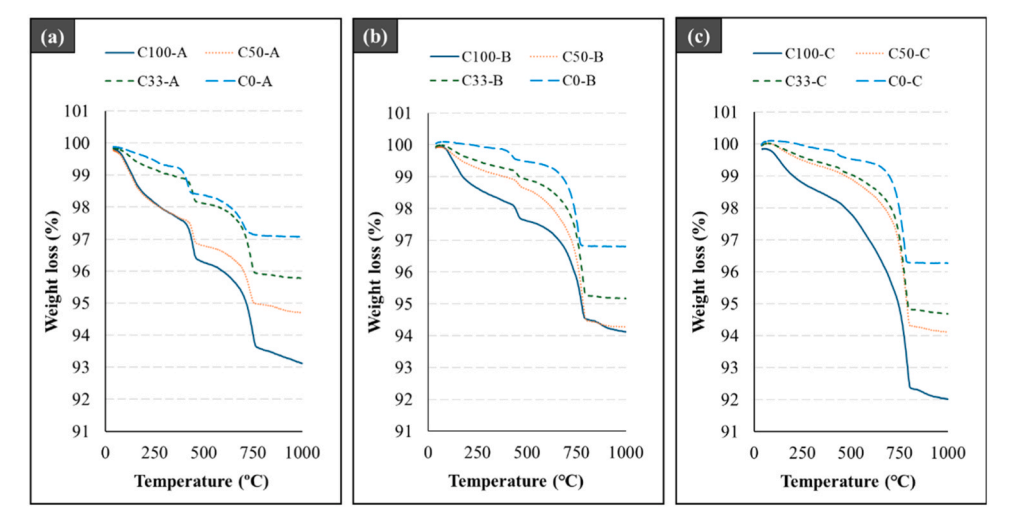
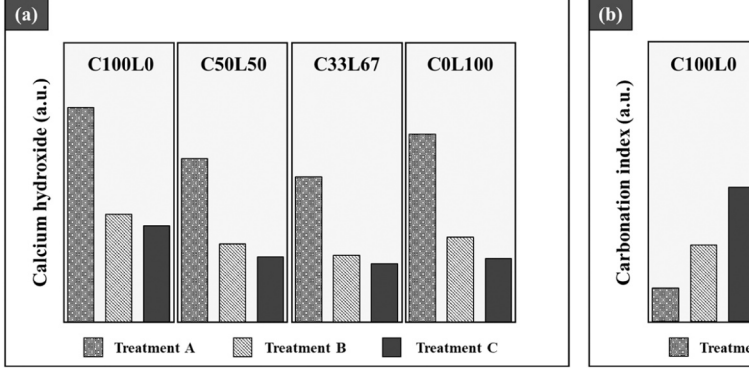


Fig. 6. Thermogravimetric results of (a) treatment A, (b) treatment B, and (c) treatment C.



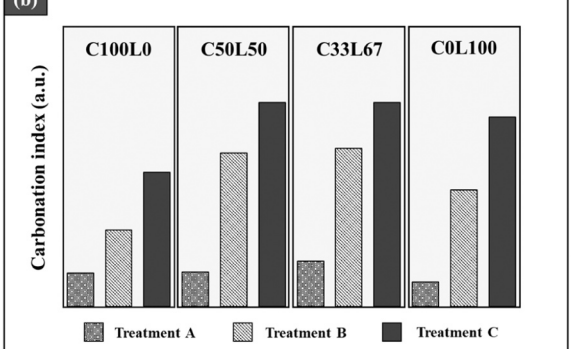


Fig. 7. Semi-quantitative assessment of (a) calcium hydroxide content and (b) a carbonation index, based on the thermogravimetric results.

According to Fig. 7a, a decreasing trend in calcium hydroxide content is observed when comparing treatments A and B. Although both groups were cured under similar environmental conditions, specimens from treatment B were cured for 91 days (compared to 28 days for treatment A), allowing more time for carbonation. A decrease in calcium hydroxide is also observed when comparing treatments B and C. In this case, the higher $\rm CO_2$ concentration in treatment C (1 % *versus* 0.04 % for treatment B) accelerated the consumption of calcium hydroxide despite the shorter curing time. Hence, treatment C appears to promote both faster and more extensive carbonation than treatments A and B, consistent with the trends observed in the compressive strength and phenolphthalein results. These observations are further supported by Fig. 7b, which shows that the carbonation index increases from A to B to C (A < B < C).

The low index observed in all groups under treatment A (Fig. 7b) indicates that carbonation was limited within the 28-day curing period. For the air lime-containing groups, this trend can be attributed to lime's high water retention capacity. According to the literature [14,32], lime's high specific surface area combined with the porosity between its calcium hydroxide crystals enables it to trap water molecules. This retained moisture delays both the evaporation of excess water and the desaturation of pores, thereby limiting $\rm CO_2$ ingress and carbonation. This behavior was also reported in a previous study [33], where air lime-containing mixtures exhibited water retention values above 90 %, suggesting strong resistance to early-age water loss. In contrast, the low carbonation index observed in the pure cement group may be explained by its lower permeability, which hinders the ingress of $\rm CO_2$ and restricts carbonation progress. As confirmed by Munhoz *et al.* [33], cement

mortars are less "breathable" as air lime-containing mortars. This behavior was also reported by Manoharan and Umarani [34].

Treatment B exhibited higher carbonation indices than treatment A, as shown in Fig. 7b. These results suggest that the influence of air lime's water retention capacity diminished over time, confirming that water retention is primarily an early-age property. As a result, the longer curing period in treatment B allowed gradual moisture loss, which facilitated CO_2 ingress and led to higher carbonation indices. This trend is consistent with the compressive strength and phenolphthalein results.

In treatment B, the influence of air lime's water retention capacity also helps explain why carbonation indices were more pronounced in the lime-cement groups than in the pure lime group. In this case, air lime's water retention capacity supported continued cement hydration while gradually promoting pore desaturation, which facilitated ${\rm CO_2}$ ingress and accelerated carbonation. This interaction between lime and cement was also reported by Cizer [32].

According to Cizer [32], this collaborative effect between air lime and cement persists only until pore water levels drop to a minimum. At that point, the system shifts from collaboration to competition, with hydration, carbonation, and evaporation competing for the remaining moisture. According to the author, a competition between hydration and carbonation is generally uncommon in lime–cement systems, as hydration tends to occur much faster than carbonation under natural conditions. Yet, under low-RH environments (such as the 55 % RH used to store the specimens), competition for moisture can occur. Research on this topic remains scarce [32] and was briefly noted in Munhoz *et al.* [33].

Treatment C (Fig. 7b) exhibited behavior similar to treatment B, with

even higher carbonation indices. This trend suggests that increasing the CO_2 concentration to 1 % for 28 days was sufficient to surpass the extent of carbonation achieved under natural conditions over 91 days (treatment B). These results are consistent with the compressive strength and carbonation depth measurements, where the highest values were also observed in the groups under treatment C.

As the carbonation indices from treatment C were more pronounced in lime-cement groups, it can be inferred that the interaction between lime and cement followed a progression similar to that observed in treatment B. This time, however, the pure lime group exhibited carbonation indices comparable to those of the lime-cement groups, indicating that the influence of water retention is minimized under accelerated conditions, contributing to a deeper carbonation front in all lime-containing groups.

3.2. Length change

After determining the compressive strength of the specimens, the next step was to measure the length change behavior of unloaded companion specimens. Since environmental conditions strongly influence length change, parameters such as relative humidity, $\rm CO_2$ concentration, and temperature were continuously monitored and kept constant throughout the tests. This control is particularly important for air lime-containing mortars, which, due to their intrinsic water retention capacity, initially retain excess water.

Retained excess water makes air lime-containing mortars more sensitive to environmental fluctuations, which can influence water evaporation. For instance, the gradual loss of moisture promotes pore desaturation and facilitates CO_2 ingress, thereby enhancing carbonation and its impact on dimensional change. Because water in air lime mortars does not serve a hydrating role but is added primarily to improve workability [11,30] evaporation becomes a key driver of length change deformations [34,35].

The overall length change behavior for each treatment is shown in Fig. 8a–c. Positive values correspond to shrinkage, while negative values

correspond to expansion. Specimens under treatment A were monitored for 56 days after curing due to technical limitations, whereas those under treatments B (Fig. 8b) and C (Fig. 8c) were monitored for 240 days.

According to Fig. 8a (treatment A), the groups containing air lime (C50L50, C33L67, and C0L100) exhibited lower shrinkage strains because they were cured under the same relative humidity as the test conditions (55 \pm 5 % RH). In contrast, C100L0 showed the highest shrinkage values. This behavior was expected because, as shown in Fig. 1, this group was initially cured in a humid chamber (95 \pm 5 % RH) and then transferred to a dry room (55 \pm 5 % RH) for the length change and creep tests, in accordance with EN 459–2:2021 [20]. Although this procedure follows the standard, it hinders a fair comparison with the other groups. Therefore, to ensure comparability, all specimens in treatments B and C were cured under the same environmental conditions.

Fig. 8a suggests that length change strains were proportional to the lime content. This trend was consistently observed in treatments B (Fig. 8b) and C (Fig. 8c) as well and can be attributed to several factors, including the water retention capacity of air lime, the aggregate fraction in each mixture, and the effects of carbonation. Each of these factors is addressed in sequence.

- Water retention: In air lime mortars, higher water retention capacity delays moisture loss, thereby reducing shrinkage strains. Since this capacity increases with lime content, as observed by Munhoz *et al.* [33], air lime-rich mixtures tend to exhibit lower shrinkage.
- Aggregate fraction: Aggregates act as a mechanical restraint, helping
 to limit shrinkage strains [36]. Because air lime has a lower density
 than Portland cement (Table 3), air lime-rich mixtures have less
 binder per weight, resulting in a slightly greater aggregate fraction
 (despite the same volumetric ratio being maintained), which reduces
 shrinkage.
- Carbonation: The carbonation of air lime is an expansive reaction that can counteract shrinkage strains caused by moisture loss. The

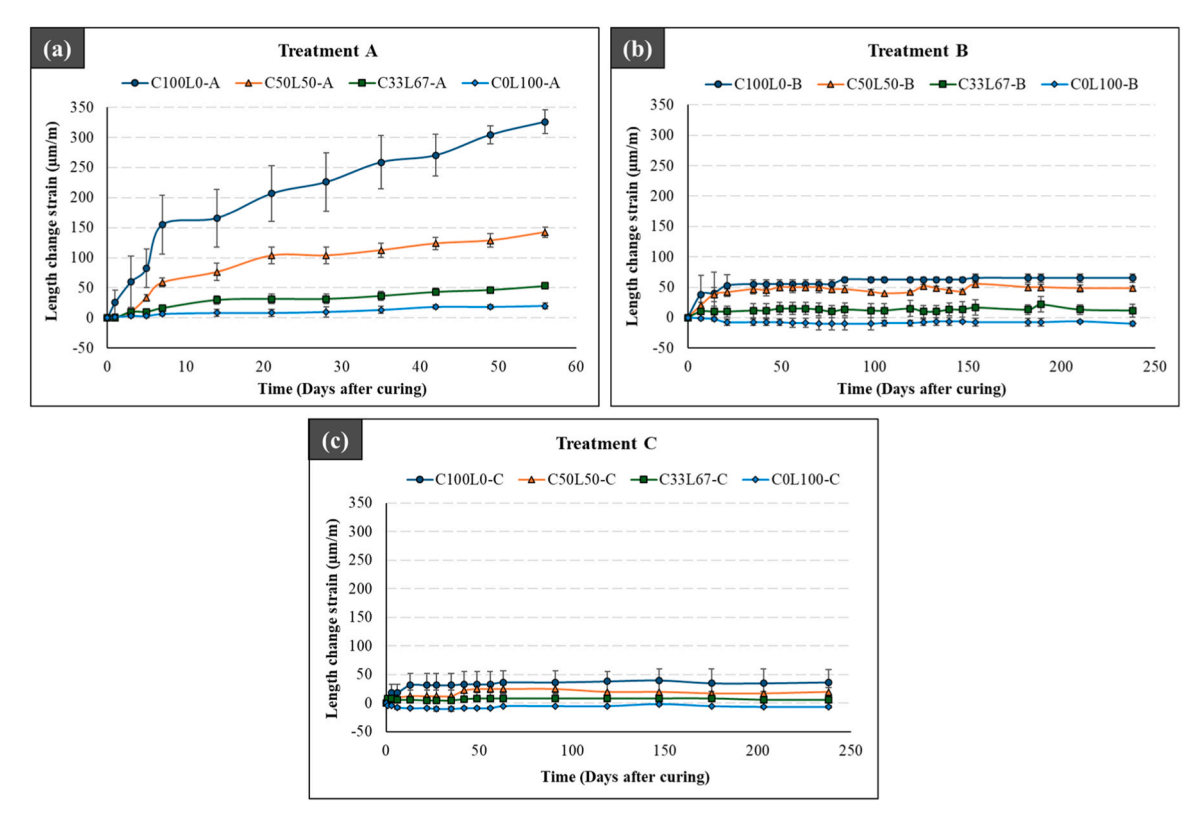


Fig. 8. Length change of mortar specimens under (a) treatment A, (b) treatment B, and (c) treatment C.

transformation of calcium hydroxide $(Ca(OH)_z)$ into calcium carbonate $(CaCO_3)$ leads to a volumetric increase of approximately 11 % (according to their molar volume). At the specimen level, however, the net expansion depends on the balance between shrinkage and carbonation, both of which are influenced by environmental conditions [37].

According to Fig. 8b-c, all groups exhibited a general stabilization trend, suggesting that most length changes occurred during the curing period and prior to the commencement of the test. Macharia [15] and Ramesh [35] also reported limited deformations over time, noting that the greatest length changes were recorded within the first month of monitoring. In this study, however, early-age measurements were not included, as the length change monitoring program was designed to align with the creep testing phase, in accordance with EN 12390–17:2019 [19]. The influence of environmental conditions on both short- and long-term length change behavior of air lime-containing mortars is currently under investigation and will be addressed in future work

Overall, Fig. 8 shows the greatest length changes in treatment A, followed by treatments B and C, with minor differences between the latter two. This behavior aligns with the previous carbonation trends, suggesting that at higher degrees of carbonation, the expansion associated with the conversion of calcium hydroxide into calcium carbonate may have gradually counteracted shrinkage tendencies over time.

Based on these observations, an important clarification must be made. The calculation of creep according to EN 12390–17:2019 [19] requires subtracting strains due to length change, as shown in Eq. (1). While this assumption is appropriate for Portland cement mortars, it may not adequately reflect the potential expansive behavior of air lime-containing mortars. In such cases, although Eq. (1) remains valid, the interpretation of $\varepsilon_{lc}(t,t_0)$ must account for the sign convention established in EN 12390–16:2019 [24]. According to the standard, shrinkage is conventionally represented as positive (thus, subtracted from total strain), whereas expansion is represented as negative. When inserted into Eq. (1), the negative expansion becomes an additive term and potentially lead to an overestimation of the total creep component. Therefore, careful attention must be paid to the sign conventions. For clarity and consistency, this study proposes using the absolute value of the length change, $|\varepsilon_{lc}(t,t_0)|$.

$$\varepsilon_{cc}(t, t_0) = \varepsilon_{cc}(t) - \varepsilon_{lc}(t, t_0) - \varepsilon_{il}(t_0)$$
(1)

in which ϵ_{cc} is the strain in the loaded specimen at the initial (t₀) or any subsequent given time (t); ϵ_{lc} is the strain due to length change (i.e., shrinkage or expansion) in the unloaded companion specimen, measured from the time of loading; ϵ_{il} is the instantaneous elastic strain measured immediately after loading.

3.3. Creep behavior

The time-dependent response of air lime-containing mortars under sustained load is presented in this section. After establishing the compressive strength (which determined the applied stress) and accounting for length change deformations, the analysis now focuses on the evolution of strain over time. Results are presented in two parts: (i) instantaneous and total strain, and (ii) total creep and elastic modulus.

3.3.1. Instantaneous and total strain

The instantaneous strain was determined from the total strain curves. These curves were obtained by loading the specimens at 30 % of their 28-day (treatments A and C) or 91-day (treatment B) compressive strength, with the corresponding loads summarized in Table 7. The total strain response is plotted in Fig. 9a-c.

A vertical line at 56 days was added to Fig. 9b-c to facilitate visualization and support comparisons with Fig. 9a (treatment A). Treatment

A was monitored for 56 days because an additional strength test revealed a substantial increase in compressive strength across all groups, which compromised the assumption of constant load required for creep testing. Therefore, treatment A was discontinued after 56 days of total strain monitoring, highlighting a particularly relevant finding for the testing of air lime—containing mortars: the absence of a reference testing age.

To the best of the authors' knowledge, no recommendations regarding a reference testing age for air lime-containing mortars are available in the literature. Thus, the results from treatment A (Fig. 9a) indicate that, under natural environmental conditions, strength-dependent properties such as creep should not be assessed before 91 days of curing. Prior to this stage, strength development due to carbonation is still ongoing and may compromise the assumption of constant load. When compressive strength was reassessed at 182 days, the variation relative to the 91-day strength was within a 5 % margin for all groups, indicating that strength had effectively stabilized by then.

According to Fig. 9a–c, small variations can be observed in all total strain curves. These fluctuations may be attributed to minor load oscillations or minor fluctuations in temperature or relative humidity. As previously mentioned, environmental conditions were maintained at $(21\pm2)\,^{\circ}\text{C}$ and $(55\pm5)\,^{\circ}\text{M}$ RH, and creep loads were automatically controlled via a hydraulic system. Although the curves in Fig. 9a-c are not directly comparable because each group and treatment was subjected to a different loading condition, they remain suitable for determining the instantaneous strain.

In this study, the instantaneous strain was determined from the linear portion of each curve (Fig. 9a-c), up to the moment when the target load (30 % of the compressive strength) was reached. A linear regression was applied to isolate the elastic response and minimize the influence of initial settling effects (transient behaviors that occur when the specimen is first subjected to loading). The corresponding fitting equations and R^2 values for each group and treatment are presented in Table 8, along with the instantaneous strain.

To facilitate comparison between groups and treatments, the instantaneous strain compliance was calculated and is presented in Table 9. Compliance is defined as the ratio of strain to stress and describes the material's tendency to deform under load. In this study, it is expressed in $\mu\epsilon/MPa$, representing the microstrain produced per unit of applied stress. A higher compliance corresponds to increased deformability.

Table 9 indicates that the strain-to-stress ratio varied proportionally with the air lime content in the mixture, suggesting that air lime-rich mixtures are more deformable than cement-rich ones, consistent with findings reported in the literature [38,39]. However, an exception was observed in Treatment C, where Colloo specimens exhibited lower compliance than C33L67. In this case, secondary effects related to the extent of non-uniform carbonation appear to have influenced the instantaneous strain of air lime-rich mortars.

The extent and uniformity of carbonation both play critical roles in governing the deformability of lime-based mortars. As carbonation progresses, calcium carbonate precipitates within the pore network, leading to microstructural densification, reduced total porosity, and increased stiffness, as reported by Lawrence [40]. However, when carbonation proceeds non-uniformly, localized precipitation disrupts the pore structure and ultimately compromise mechanical performance.

Table 7Creep loads and corresponding standard deviations according to each group and treatment.

Groups	Treatment A (kN)	Treatment B (kN)	Treatment C (kN)
C100L0	60.21 ± 0.09	$\textbf{75.22} \pm \textbf{0.90}$	83.51 ± 0.37
C50L50	21.60 ± 0.61	23.39 ± 0.31	26.46 ± 0.23
C33L67	$\textbf{8.34} \pm \textbf{0.42}$	10.09 ± 0.32	12.19 ± 0.46
C0L100	0.88 ± 0.07	2.19 ± 0.06	3.03 ± 0.17

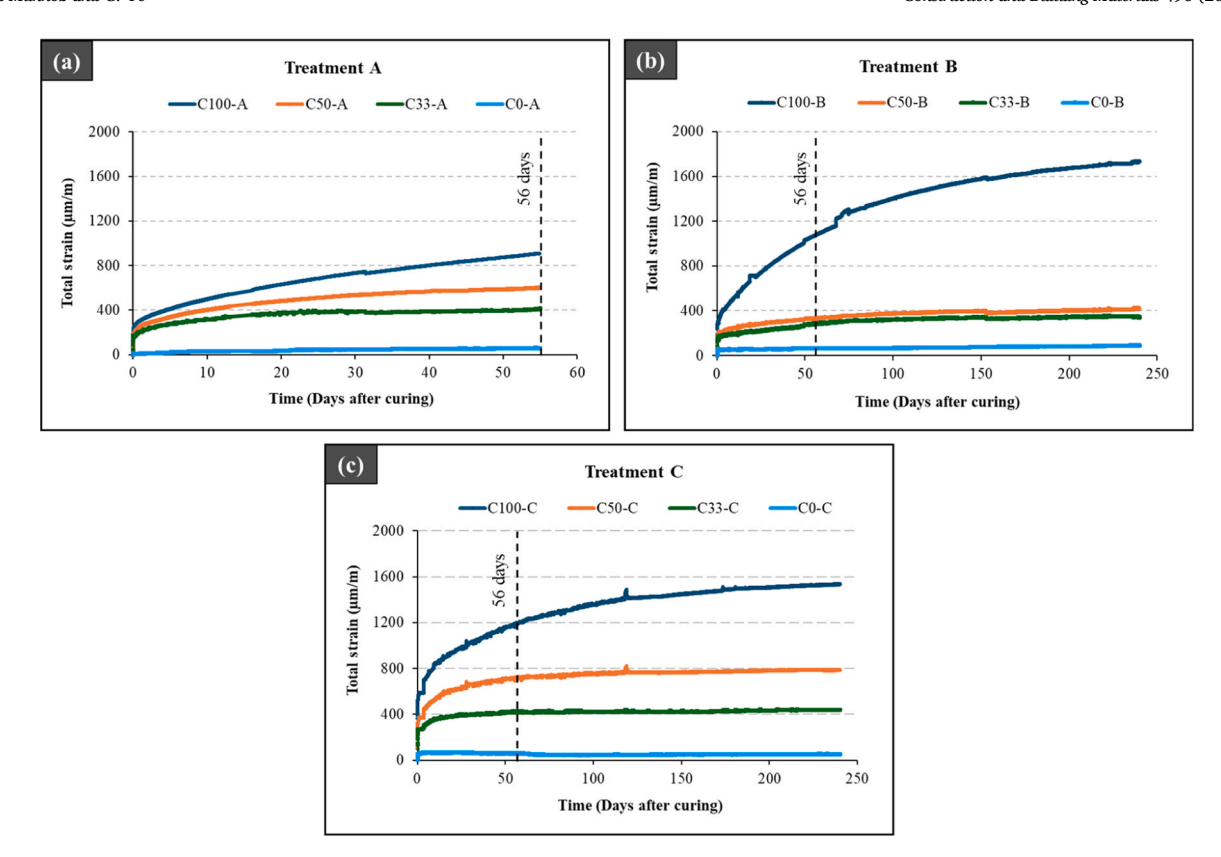


Fig. 9. Total strain of mortar specimens cured under (a) treatment A, (b) treatment B, and (c) treatment C.

Table 8
Instantaneous strain due to loading according to each group and treatment.

Groups	Equation	R ²	Instantaneous strain (µm/m)
Treatment A C100L0	$y = 1.3726 \bullet x + 1.4378$	0.997	213.65
Treatment A C50L50	$y = 0.5702 \bullet x + 2.2733$	0.991	165.79
Treatment A C33L67	$y = 0.3464 \bullet x + 0.2814$	0.975	111.56
Treatment A C0L100	$y = 0.1522 \bullet x + 0.0101$	0.990	27.26
Treatment B C100L0	$y = 1.5183 \bullet x + 4.4779$	0.988	229.97
Treatment B C50L50	$y = 0.6344 \bullet x + 3.1638$	0.990	159.49
Treatment B C33L67	$y = 0.3485 \bullet x + 1.0120$	0.977	128.38
Treatment B C0L100	$y = 0.1917 \bullet x + 0.3373$	0.970	48.32
Treatment C C100L0	$y = 1.1089 \bullet x + 5.0518$	0.998	353.95
Treatment C C50L50	$y = 0.5255 \bullet x + 1.4594$	0.996	235.02
Treatment C C33L67	$y = 0.2854 \bullet x + 0.2648$	0.996	212.42
Treatment C C0L100	$y = 0.3606 \bullet x + 0.4890$	0.979	32.04

According to Padmaraj and Arnepalli [41], once microstructural densification reaches an optimum limit, continued precipitation of calcium carbonate can create internal stresses that lead to microcracking, thereby increasing total porosity and deformability. This effect is reflected in Table 9, where treatment C (associated with a greater carbonation extent than treatments A and B) generally shows the highest instantaneous strain compliance. Phenolphthalein testing, thermogravimetric analysis, and compressive strength results from previous

Table 9
Instantaneous strain compliance according to each group and treatment.

Groups	Treatment A (με/MPa)	Treatment B (με/MPa)	Treatment C (με/MPa)
C100L0	35.56	30.95	42.36
C50L50	78.28	68.16	89.84
C33L67	139.27	128.89	171.45
C0L100	324.57	220.65	106.81

sections support these hypotheses. Once again, C0L100 was the exception to the overall trend, showing decreasing compliance from treatment A to C. Its higher porosity likely allowed calcium carbonate to precipitate without inducing microcracking. Thus, densification never reached the optimum limit observed in the cement–containing mixtures. Further pore structure characterization is recommended.

3.3.2. Total creep and elastic modulus

The following plots (Figs. 10–13) present the time-dependent strain for each group (C100L0, C50L50, C33L67, and C0L100) and treatment (A, B, and C). Each strain component measured in this study (length change strain, total strain, instantaneous strain, and the resulting total creep strain) is expressed as compliance ($\mu\epsilon$ /MPa). Due to the ongoing strength development discussed in the previous section, monitoring of all groups under treatment A was interrupted after 56 days. The results for the pure cement group, C100L0, are shown in Fig. 10a-c.

C100L0 specimens under treatment A were cured at 95 % RH for 28 days and then transferred to a 55 % RH environment for the creep test, in accordance with EN 12390–17:2019 [19]. However, this change in environment introduced a humidity gradient that led to the increased shrinkage strains observed in Fig. 10a. To avoid this issue, specimens under treatments B and C were cured at 55 % RH.

Despite the longer curing period and consistent environmental conditions, specimens under treatment B (Fig. 10b) still exhibited a similar

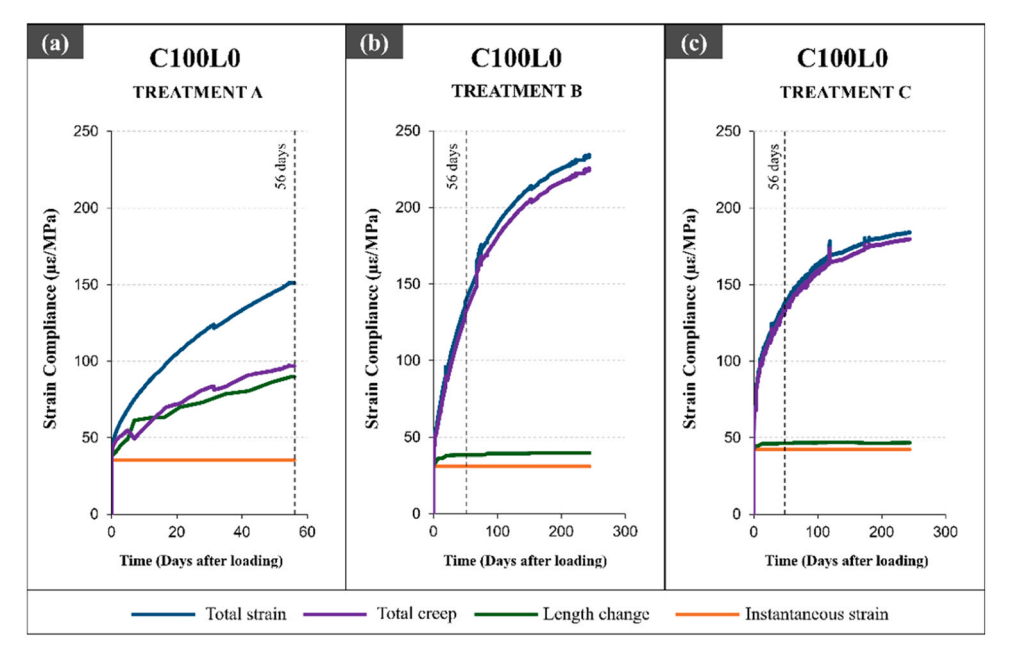


Fig. 10. Deformation behavior of C100L0 according to (a) Treatment A; (b) Treatment B; and (c) Treatment C.

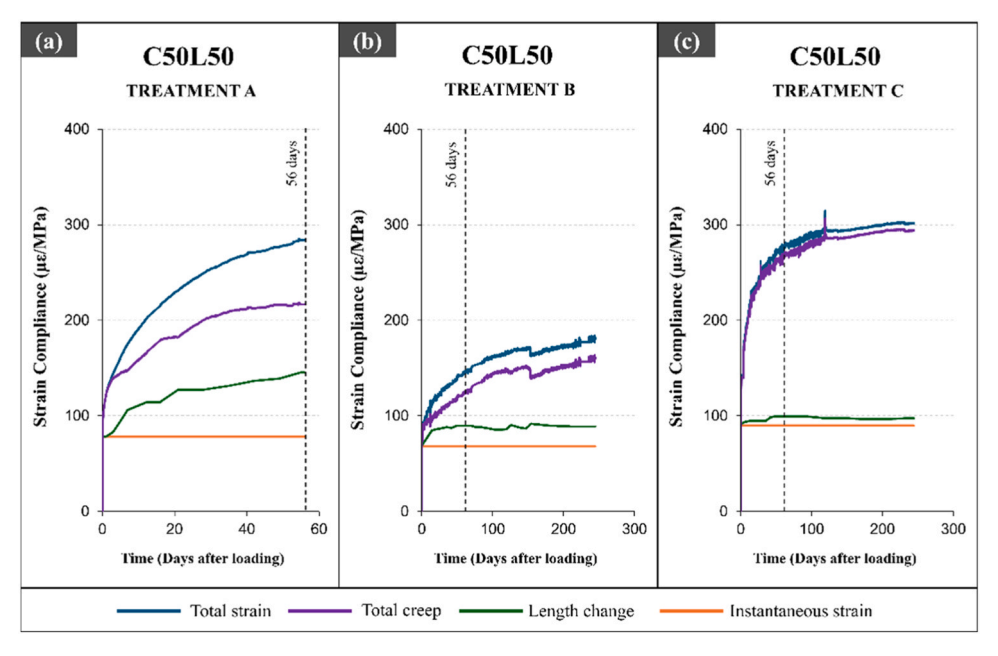


Fig. 11. Deformation behavior of C50L50 according to (a) Treatment A; (b) Treatment B; and (c) Treatment C.

instantaneous strain (30.95 $\mu\epsilon/MPa)$ to those under treatment A (35.56 $\mu\epsilon/MPa)$. This indicates that instantaneous strain was primarily governed by mixture composition, which remained unchanged across treatments. The slightly lower value observed in treatment B can be explained by the longer curing period and the associated matrix consolidation.

Compared to treatment B, specimens under treatment C (Fig. 10c) exhibited lower total creep compliance, suggesting that accelerated carbonation curing and the extensive precipitation of calcium carbonate densified the matrix, thereby increasing stiffness and limited long-term deformation under sustained load. In contrast, treatment C showed the highest instantaneous strain among the three treatments (42.36 $\mu\epsilon/MPa$), supporting the earlier hypothesis that extensive precipitation of calcium carbonate, while enhancing stiffness, can also generate internal stresses when porosity is limited. A detailed characterization of

the pore structure is recommended to support this discussion.

C50L50 results are shown in Fig. 11. Specimens cured under treatment A (Fig. 11a) exhibited greater length change and total creep strains than those in treatment B (Fig. 11b). The presence of uncarbonated lime, which reduces stiffness and increases susceptibility to time-dependent deformation, may explain the higher strains observed in treatment A. In contrast, the reduced strains in treatment B are consistent with its longer curing period and greater carbonation extent, as reported in the previous sections.

The highest instantaneous strain was observed in treatment C (89.83 $\mu\epsilon/MPa$, Fig. 11c). This behavior can be attributed to accelerated carbonation and the extensive precipitation of calcium carbonate, which enhance stiffness but also generate internal stresses when porosity is limited, thereby promoting microstructural cracking. A similar trend was observed in C100L0 (Fig. 10). The extensive precipitation of

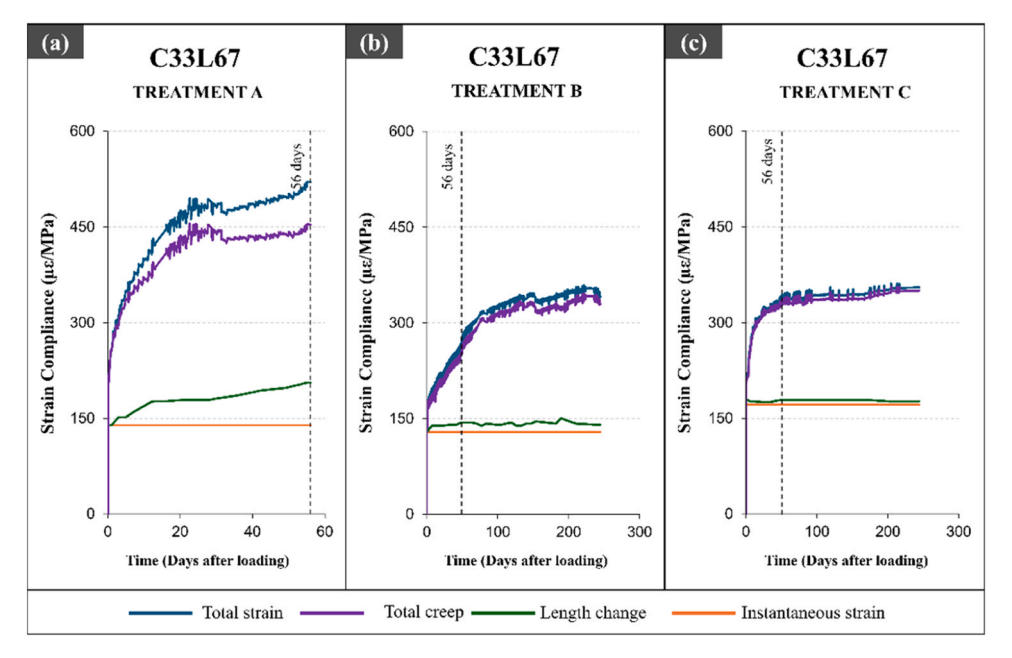


Fig. 12. Deformation behavior of C33L67 according to (a) Treatment A; (b) Treatment B; and (c) Treatment C.

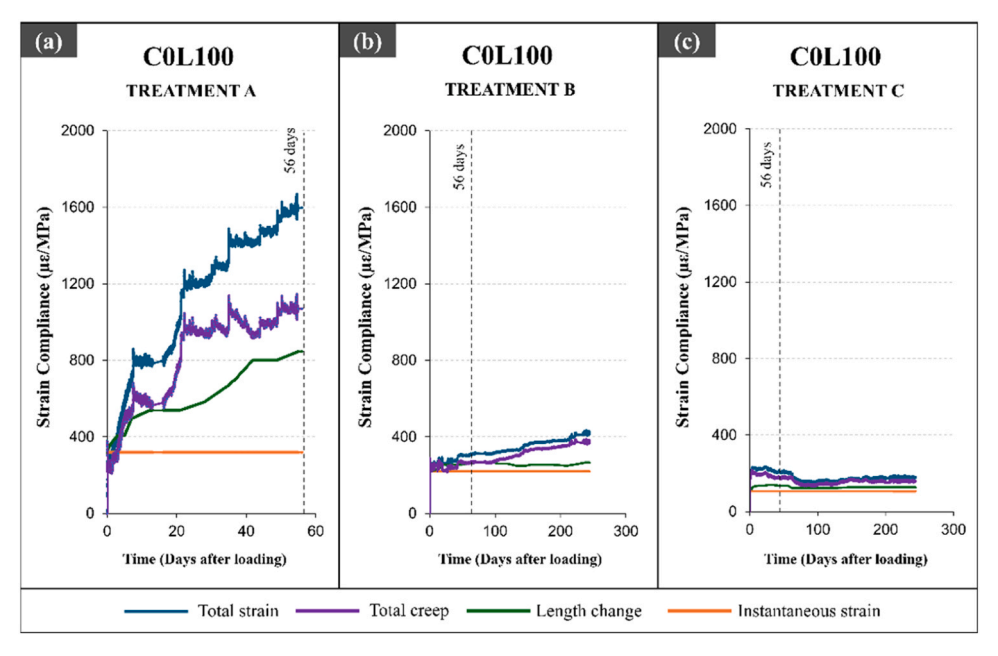


Fig. 13. Deformation behavior of COL100 according to (a) Treatment A; (b) Treatment B; and (c) Treatment C.

calcium carbonate in treatment C was confirmed by phenolphthalein and TG tests.

Results for the other lime-cement group, C33L67, are shown in Fig. 12. Unlike C50L50, the C33L67 specimens exhibited their highest strain values under treatment A (Fig. 12a). This behavior suggests that the higher air lime content, which intrinsically increases matrix softness [39], combined with the short curing period under natural conditions (28 days at $0.04 \% CO_2$), resulted in limited carbonation and a more pronounced deformation response.

Specimens under treatment B (Fig. 12b) exhibited a significant reduction in all strain components compared to those in treatment A. This reduction indicates that the longer curing period led to a greater extent of carbonation, which consolidated both the microstructure and the strain response. The slightly lower instantaneous strain compliance observed in treatment B aligns with the trends seen in C100L0 (Fig. 10)

and C50L50 (Fig. 11). In these cases, instantaneous strain was primarily governed by mixture composition, with curing conditions playing a minor role.

Specimens under treatment C (Fig. 12c) reached total strain compliance magnitudes similar to those under treatment B, yet their total strain curves differed considerably. While the curve from treatment B showed a gradual increase over time, the curve from treatment C showed a sharp early rise. This distinct response suggests that specimens in treatment C underwent microstructural adjustments (e.g., initial settling), which contributed to the increased early-age deformation. The high instantaneous strain observed in treatment C (171.46 $\mu\epsilon/MPa$) supports this interpretation.

Such early-age adjustments could be attributed to (i) the irregular carbonation front and formation of Liesegang rings, revealed during the phenolphthalein test (Fig. 5); and (ii) excessive precipitation of calcium

carbonate, which can generate internal stresses when porosity is limited. Nevertheless, after this initial adjustment, the strain evolution in treatment C remained relatively stable, consistent with the behavior expected from a denser, stiffer matrix formed through accelerated carbonation curing.

The outcomes for the final and most air lime-rich group, COL100, are presented in Fig. 13. As the group with the lowest mechanical strength, COL100 was particularly sensitive to microstructural changes, which may also explain the pronounced oscillations recorded over time. The pure lime group also exhibited a less uniform deformation response than the others, potentially due to the irregular carbonation front revealed by the phenolphthalein test (Fig. 5).

The specimens under treatment A (Fig. 13a) were tested after 28 days of curing, when carbonation was still at an early stage, resulting in notably high total strains. Unlike Portland cement mortars, these findings indicate that air lime-rich mortars cured under natural conditions require more than 28 days to develop sufficient strength. For instance, specimens under treatment B (Fig. 13b), cured for 91 days, exhibited substantially lower deformation than those under treatment A.

Specimens under treatment B (Fig. 13b) also showed lower instantaneous strain compliance, confirming that instantaneous strain is governed primarily by mixture composition and secondarily by curing conditions, a pattern consistently observed across all groups (C100L0, C50L50, and C33L67). In treatment C (Fig. 13c), however, strain decreased, contrasting with the trend observed in other groups cured under increased $\rm CO_2$ concentrations. This behavior suggests that, in this case, accelerated carbonation curing promoted matrix consolidation without inducing internal stresses that could lead to microstructural cracking, thereby explaining the lowest instantaneous strain compliance observed in Fig. 13c. Nonetheless, C0L100's total strain did not follow the typical curves often reported for Portland cement-containing mortars.

Under treatment A (Fig. 13a), the total creep compliance curve initially shows a progressive increase, followed by temporary stabilization and a subsequent increase. This atypical behavior reflects the immature state of the COL100 matrix at the time of testing. As previously discussed, after 28 days of natural curing, carbonation was still incomplete. As a result, the pure air lime mortars were mechanically underdeveloped and prone to continued microstructural adjustments.

Under treatment B (Fig. 13b), C0L100 specimens exhibited less irregular behavior than in treatment A, highlighting the benefits of an extended curing period. In this case, strength development was no longer a significant concern (as in treatment A), and most of the erratic behavior observed in Fig. 13b was limited to the first days of testing. This observation suggests that initial settling is a relevant issue in the creep monitoring of air lime-rich mortars, even after prolonged curing.

The specimens under treatment C (Fig. 13c) also exhibited a non-traditional creep curve, where initial settling may explain the early-age strain increase. However, because this group was subjected to accelerated carbonation curing, the specimens likely continued to benefit from internal $\rm CO_2$ availability, extending the carbonation process beyond curing and altering the creep response. This pattern explains the plateau followed by a decrease in strain observed in Fig. 13c. The increased length change associated with expansion due to carbonation supports this interpretation. After this transient phase, the strain curve rose again, suggesting that creep was still developing. A longer monitoring is needed to confirm this behavior.

In addition to the evaluation of total strain and creep performance, the secant elastic modulus was determined to characterize the stiffness of each group and to provide a complementary perspective on their deformation behavior. The results are summarized in Table 10.

The results shown in Table 10 indicate that the secant elastic modulus was proportional to the cement content, with C100L0 exhibiting the highest values. This trend was expected and is consistent with the compressive strength and total strain compliance results.

Among the different treatments, Table 10 shows that specimens

Table 10
Secant elastic modulus measured for each group and treatment.

Groups	Treatment A (GPa)	Treatment B (GPa)	Treatment C (GPa)
C100L0	17.49 ± 1.92	18.93 ± 2.50	17.54 ± 2.45
C50L50	7.16 ± 0.44	9.31 ± 1.05	8.57 ± 0.88
C33L67	3.18 ± 0.31	5.47 ± 0.81	4.53 ± 0.69
C0L100	0.46 ± 0.07	3.72 ± 0.39	1.95 ± 0.23

under treatment B (extended curing under natural conditions) exhibited the highest secant elastic modulus. This outcome can be attributed to the prolonged curing period, which promoted both cement hydration and air lime carbonation, leading to greater microstructural consolidation. In contrast, specimens cured under treatment A showed the lowest elastic modulus. This behavior can be explained by the short curing period under natural conditions, which restricted carbonation and microstructural consolidation, particularly in the air lime-containing groups.

Finally, specimens under treatment C (short curing in an accelerated carbonation environment) indicate that, while forced carbonation contributed to matrix densification through the precipitation of calcium carbonate, it also appears to have generated internal stresses that led to microstructural cracking, thereby lowering the secant elastic modulus. This impairment was less evident in cement-rich groups, where higher global stiffness may have mitigated the effects of microstructural cracking, limiting the reduction in elastic modulus. This interpretation is further supported by the instantaneous strain compliance.

4. Conclusions

This study measured the total creep of air lime-containing mortars over a period of up to 240 days. Four groups (C100L0, C50L50, C33L67, and C0L100) were monitored under three distinct curing treatments, and complementary tests (compressive strength, phenolphthalein, TGA, length change, and secant elastic modulus) were performed. A summary of the findings is presented below:

- Compressive strength: The air lime content was inversely proportional to the compressive strength, with C100L0 exhibiting the highest values. Among the curing treatments, the 28-day accelerated carbonation curing (treatment C) showed the highest strength values, followed by the 91-day natural curing (treatment B). These results indicate that air lime-containing mortars require prolonged curing under natural conditions (or carbonation-promoting environments) to achieve significant strength levels;
- 2) The role of carbonation: The air lime content was directly proportional to the carbonation depth. Among the treatments, the accelerated carbonation curing (treatment C) produced the greatest carbonation depths, followed by the prolonged natural curing (treatment B). In air lime groups, the presence of Liesegang rings revealed an irregular carbonation pattern that may impair mechanical performance. Moreover, the phenolphthalein test could not accurately determine the carbonation depth in air lime-rich groups, as TG analyses indicated a systematic tendency toward overestimation.
- 3) Length change strains: The expansive carbonation of air lime-rich mortars mitigated shrinkage tendencies, with C0L100 generally exhibiting the lowest strains. Treatments B and C consistently showed lower length change strains compared to treatment A, reflecting the benefits of extended and accelerated carbonation curing in improving volume stability.
- 4) **Instantaneous and total strain:** Instantaneous strain was governed primarily by mixture composition, with curing conditions playing a secondary role. Air lime-rich mixtures exhibited higher strains than cement-rich ones, reflecting their lower stiffness. Specimens under treatment B generally showed the lowest instantaneous strain

- compliances, while those under treatment C exhibited the highest values. Although accelerated carbonation densifies the matrix and reduces long-term creep, excessive precipitation of calcium carbonate (beyond a porosity-dependent threshold) can generate internal stresses that promote microstructural cracking and increase instantaneous strain.
- 5) Total creep and elastic modulus: Cement-rich mixtures consistently showed lower creep strains due to higher stiffness and strength, whereas air lime-rich mixtures were more deformable and prone to microstructural adjustments. This was confirmed by the secant elastic modulus results, with C100L0 exhibiting the highest values. Pure lime (C0L100) showed a distinct creep behavior, with immature matrices (treatment A) and initial settling effects (treatments B and C) responsible for the non-traditional creep curves observed in this study.

Finally, to ensure the reliable application of EN 12390–17 to air lime-containing mortars, three adjustments are recommended: (i) adopting a minimum curing age of 91 days under natural conditions (or an equivalent maturity criterion), since strength development continues beyond 28 days; (ii) revising the calculation of creep to explicitly account for length change strains due to both expansion and shrinkage, with an adjusted sign convention; and (iii) defining recommended load levels that minimize the influence of initial settling effects in soft mortars. Together, these adjustments would allow EN 12390–17 to be applied more reliably to air lime-containing mortars, bridging the gap between current standards and the specific behavior of non-hydraulic binders.

CRediT authorship contribution statement

Guilherme da Silva Munhoz: Writing – original draft, Visualization, Methodology, Investigation, Formal analysis, Conceptualization. **Guang Ye:** Writing – review & editing, Supervision, Methodology, Conceptualization.

Declaration of Competing Interest

The authors declare that they have no known competing financial interests or personal relationships that could have appeared to influence the work reported in this paper.

Acknowledgments

This research has been carried out within the framework of the EU SUBLime network. This Project has received funding from the European Union's Horizon 2020 research and innovation programme under Marie Sklodowska-Curie project SUBLime [Grant Agreement no955986].

Data availability

Data will be made available on request.

References

- [1] D. Carran, J. Hughes, A. Leslie, C. Kennedy, A short history of the use of lime as a building material beyond Europe and North America, Int. J. Archit. Herit. 6 (2012) 117–146, https://doi.org/10.1080/15583058.2010.511694.
- [2] R. Veiga, Air lime mortars: what else do we need to know to apply them in conservation and rehabilitation interventions? A review, Constr. Build. Mater. 157 (2017) 132–140. https://doi.org/10.1016/j.conbuildmat.2017.09.080.
- [3] D. Vasovic, J. Terzovic, A. Kontic, R. Okrajnov-Bajic, N. Sekularac, The influence of water/binder ratio on the mechanical properties of lime-based mortars with White portland cement, Crystals 11 (2021) 958, https://doi.org/10.3390/cryst11080958.
- [4] P.K. Mehta, P.J.M. Monteiro. Concrete: Microstructure, Properties and Materials, third ed., McGraw Hill, New York, 2006.
- [5] K. Scrivener, F. Martirena, S. Bishnoi, S. Maity, Calcined clay limestone cements (LC3), Cem. Concr. Res. 114 (2018) 49–56, https://doi.org/10.1016/j. cemconres.2017.08.017.

- [6] B. Sun, G. Ye, G. De Schutter, A review: reaction mechanism and strength of slag and Fly ash-based alkali-activated materials, Constr. Build. Mater. 326 (2022) 126843, https://doi.org/10.1016/j.conbuildmat.2022.126843.
- [7] Z. Liu, C. Lv, F. Wang, S. Hu, Recent advances in carbonatable binders, Cem. Concr. Res. 173 (2023) 107286, https://doi.org/10.1016/j.cemconres.2023.107286.
- [8] A. Arizzi, G. Cultrone, Negative effects of the use of White portland cement as additive to aerial lime mortars set at atmospheric conditions: a chemical, mineralogical and physical-mechanical investigation, in: S.M. Rivera, A.L.P. Diaz (Eds.), Brick and Mortar Research, first ed., Nova Science Publishers, 2013, pp. 231–243.
- [9] M.A. Oliveira, M. Azenha, P.B. Lourenço, A. Meneghini, E.T. Guimarães, F. Castro, D. Soares, Experimental analysis of the carbonation and humidity diffusion processes in aerial lime mortar, Constr. Build. Mater. 148 (2017) 38–48, https://doi.org/10.1016/j.conbuildmat.2017.04.120.
- [10] F.G. Branco, M.L. Belgas, C. Mendes, L. Pereira, J.M. Ortega, Characterization of fresh and durability properties of different lime mortars for being used as masonry coatings in the restoration of ancient constructions, Sustainability 13 (2021) 4909, https://doi.org/10.3390/su13094909.
- [11] S.H. Kang, Y.H. Kwon, J. Moon, Quantitative analysis of CO₂ uptake and mechanical properties of air lime-based materials, Energies 12 (2019) 2903, https://doi.org/10.3390/en12152903.
- [12] G. Cultrone, E. Sebastián, M.O. Huertas, Forced and natural carbonation of lime-based mortars with and without additives: mineralogical and textural changes, Cem. Concr. Res. 35 (2005) 2278–2289, https://doi.org/10.1016/j.cem.concres.2004.12.012.
- [13] Ö. Cizer, K. Van Balen, D. Van Gemert, Competition between hydration and carbonation in hydraulic lime and lime–pozzolana mortars, Adv. Mater. Res. 133–134 (2010) 241–246, https://doi.org/10.4028/www.scientific.net/amr.133-134.241.
- [14] S. Pavía, M. Aly, Influence of aggregate and supplementary cementitious materials on the properties of hydrated lime (CL90s) mortars, Mater. Constr. 66 (2016) e104, https://doi.org/10.3989/mc.2016.01716.
- [15] S.M. Macharia, Creep mechanisms in cement and lime mortared masonry (Doctoral thesis), University of Bath, 2015.
- [16] J.J. Brooks, B.H.A. Bakar, Shrinkage and creep of masonry mortar, Mater. Struct. 37 (2004) 177–183, https://doi.org/10.1007/bf02481617.
- [17] I. Papayianni, Creep deformation of lime-based repair mortars: the effect of aggregate size, in: D.R.W. Martens, A.T. Vermeltfoort (Eds.), International Brick and Block Masonry Conference, Technische Universiteit Eindhoven, Amsterdam, 2004.
- [18] E. Verstrynge, D.Van Gemert, Creep failure of two historical masonry towers: analysis from material to structure, Int. J. Mason. Res. Innov. 3 (2018) 50–71, https://doi.org/10.1504/ijmri.2018.089056.
- [19] European Committee for Standardization, EN 12390-17: Testing hardened concrete
 Part 17: Determination of creep of concrete in compression. Brussels. 2019.
- [20] European Committee for Standardization, EN 459-2: Building lime Part 2: Test methods. Brussels. 2021.
- [21] European Committee for Standardization, EN 196-1: Methods of testing cement Part 1: Determination of strength, Brussels, 2016.
- [22] European Committee for Standardization, EN 1015-11: Methods of test for mortar for masonry – Part 11: Determination of flexural and compressive strength of hardened mortar, Brussels, 2019.
- [23] European Committee for Standardization, EN 12390-3: Testing hardened concrete – Part 3: Compressive strength of test specimens, Brussels, 2019.
- [24] European Committee for Standardization, EN 12390-16: Testing hardened concrete
 Part 16: Determination of the shrinkage of concrete, Brussels, 2019.
- [25] G.S. Munhoz, G. Ye, Experimentally measured length change of air lime-containing mortars [dataset], 4TU. ResearchData, 2025. http://doi.org/10.4121/149fd8c 5-f05f-4760-9dc4-e820a76691ea.
- [26] G.S. Munhoz, G. Ye, Experimentally measured total strain of air lime-containing mortars [dataset], 4TU. ResearchData, 2025. https://doi.org/10.4121/89c32a06-3 73e-44c0-9805-8b34cac8321a.
- [27] RILEM, CPC-18: measurement of hardened concrete carbonation depth, Kluwer Acad. Publ., Cham, 1988, https://doi.org/10.1007/bf02472327.
- [28] B. Lothenbach, P. Durdziński, K.De Weerdt, Thermogravimetric analysis, in: K. Scrivener, R. Snellings, B. Lothenbach (Eds.), A Practical Guide to Microstructural Analysis of Cementitious Materials, first ed., CRC Press, Boca Raton, 2016, pp. 281–304.
- [29] European Committee for Standardization, EN 12390-13: Testing hardened concrete - Part 13: Determination of secant modulus of elasticity in compression, Brussels, 2019.
- [30] J. Lanas, J.I. Alvarez, Masonry repair lime-based mortars: factors affecting the mechanical behavior, Cem. Concr. Res. 33 (2003) 1867–1876, https://doi.org/ 10.1016/s0008-8846(03)00210-2.
- [31] C. Rodriguez-Navarro, O. Cazalla, K. Elert, E. Sebastian, Liesegang pattern development in carbonating traditional lime mortars, Proc. R. Soc. Lond. A 458 (2002) 2261–2273, https://doi.org/10.1098/rspa.2002.0975.
- [32] O. Cizer, Competition between carbonation and hydration on the hardening of calcium hydroxide and calcium silicate binders (Doctoral thesis), Katholieke Universiteit Leuven, 2009.
- [33] G.S. Munhoz, Y. Zeng, E. Schlangen, G. Ye, The water retention role in the carbonation of air lime: hero or villain? in: P.B. Lourenço, M. Azenha, J.M. Pereira (Eds.), Towards the Next Generation of Sustainable Masonry Systems: Mortars, Renders, Plasters and Other Challenges Universidade do Minho, Funchal, 2024, pp. 71–72.

- [34] A. Manoharan, C. Umarani, Properties of air lime mortar with bio-additives, Sustainability 14 (2022) 8355, https://doi.org/10.3390/su14148355.
- [35] M. Ramesh, A multi-scale approach to the study of lime-cement mortars in masonry (Doctoral thesis), Universidade do Minho, 2021.
- [36] A.R. Santos, M.R. Veiga, A. Santos Silva, J. de Brito, J.I. Álvarez, Evolution of the microstructure of lime-based mortars and influence on the mechanical behaviour: the role of the aggregates, Constr. Build. Mater. 187 (2018) 907–922, https://doi. org/10.1016/j.conbuildmat.2018.07.223.
- [37] K. Van Balen, Carbonation reaction of lime: kinetics at ambient temperature, Cem. Concr. Res. 35 (2005) 647–657, https://doi.org/10.1016/j. cemconres.2004.06.020.
- [38] S. Pavía, O. Brennan, Portland cement–lime mortars for conservation, in: J. J. Hughes, J. Válek, C.J.W.P. Groot (Eds.), Historic Mortars, first ed., Springer, Cham. 2019, pp. 129–142. https://doi.org/10.1007/978-3-319-91606-4-10.
- Cham, 2019, pp. 129–142, https://doi.org/10.1007/978-3-319-91606-4_10.
 [39] B.T. Rosson, K. Søyland, T.E. Boothby, Inelastic behavior of sand–lime mortar joint masonry arches, Eng. Struct. 20 (1998) 14–24, https://doi.org/10.1016/s0141-0296(97)00052-7.
- [40] R.M.H. Lawrence, A study of carbonation in non-hydraulic lime mortars (Doctoral thesis), University of Bath, 2006.
- [41] D. Padmaraj, D.N. Arnepalli, Mechanism of carbonation in lime-stabilized silty clay from chemical and microstructure perspectives, Int. J. Geosynth. Ground Eng. 7 (2021) 1–12, https://doi.org/10.1007/s40891-021-00318-2.